Mechanisms of curcumin-based photodynamic therapy and its effects in combination with electroporation: an in vitro and molecular dynamics study

Wojciech Szlasa[1], Anna Szewczyk[2,3], Małgorzata Drąg-Zalesińska[4], Hanna Czapor-Irzabek[5], Olga Michel[2], Aleksander Kiełbik[1], Karolina Cierluk[6], Aleksandra Zalesińska[1], Vitalij Novickij[7], Mounir Tarek[8], Jolanta Saczko[2], Julita Kulbacka[2]

1. Faculty of Medicine, Wroclaw Medical University, Wroclaw, Poland
2. Department of Molecular and Cellular Biology, Faculty of Pharmacy, Wroclaw Medical University, Wroclaw, Poland
3. Department of Animal Developmental Biology, Institute of Experimental Biology, University of Wroclaw, Wroclaw, Poland
4. Division of Histology and Embryology, Faculty of Medicine, Wroclaw Medical University, Wroclaw, Poland
5. Laboratory of Elemental Analysis and Structural Research, Wroclaw Medical University, Borowska 211A, Wroclaw 50-556, Poland
6. Faculty of Chemistry, Wroclaw University of Science and Technology, Wroclaw, Poland
7. Institute of High Magnetic Fields, Vilnius Gediminas Technical University
8. Université de Lorraine, CNRS, LPCT, F-54000 Nancy

Correspondence email: Julita.Kulbacka@umed.wroc.pl; Wojciech.Szlasa@outlook.com;

Postal address: Borowska 211A, Wroclaw 50-556, Poland

Telephone: +48 71 784 06 92
ORCID: 0000-0001-8272-5440 (Julita Kulbacka), 0000-0002-5477-5771 (Wojciech Szlasa)

Abstract:

Photodynamic therapy (PDT) and electrochemotherapy (ECT) are two methods designed to enhance the anticancer potential of various drugs. Various clinical trials proved the efficacy of both ECT and PDT in melanoma treatment. Curcumin is a natural polyphenolic compound with high anticancer potential against melanoma due to its light absorption properties and toxicity towards cancer cells; however, high reactivity and amphipathic structure of curcumin are limiting its utility. This study aimed to propose the most effective protocol for antimelanoma combination of both therapies (PDT and ECT) in the context of curcumin. The in vitro studies were carried on melanotic melanoma (A375), amelanotic melanoma (C32) and fibroblast (HGF) cell lines. In molecular dynamics studies curcumin presented the single-layer localization in the water-membrane interphase. Further, the mass spectrometry studies exposed that during the PDT treatment curcumin is degraded to vanillin, feruloylmethane, and ferulic acid. Instant ECT with curcumin followed by PDT is the most efficient approach due to its selective genotoxicity towards malignant cells. The metabolic activity of fibroblasts decreased, however, at the same time the fragmentation of DNA did not occur. Additionally, instant PDT with curcumin followed by ECT after 3 h of incubation was a therapy selective towards melanotic melanoma.

Keywords: melanoma, curcumin, photodynamic therapy, electrochemotherapy, curcumin degradation, curcumin localization

Highlights:

- Cytotoxic effect of curcumin-aided PDT might be enhanced by electroporation.
- Standalone electroporation with curcumin is not effective against melanoma cells.

- Caspase-12 is involved in the genotoxicity after curcumin-PDT combined with EP.
- Irradiation of curcumin generates anticancer derivatives, like vanillin.

1. Introduction

Curcumin is a flavonoid compound extracted from the roots of *Curcuma longa* [1]. The amphipathic molecule is characterized by a great ability to absorb blue light (~ 420 nm), high cell membrane permeability and low systemic bioavailability [2, 3]. Its antioxidative, antiproliferative and antineoplastic properties are nowadays widely analyzed on the molecular level [4, 5]. Numerous studies aim to evaluate the anticancer properties of the compound and characterize its mechanism of action, pharmacokinetic and pharmacodynamic properties [6, 7]. Introducing curcumin into the clinical practice requires a detailed examination of its metabolic, biochemical and biophysical properties.

Photodynamic therapy (PDT) is one of the therapeutic applications in which curcumin plays a role of photosensitizer [8, 9, 10, 11, 12]. By the absorption of light energy, curcumin changes electron structure and rapidly releases the energy quant, leading to the induction of the oxidative stress among cells [9]. Recent studies demonstrated that the theory has a strong laboratory validation [13, 14, 15]. The high reactivity of curcumin, combined with energetically demanding conditions of PDT, gave rise to the idea that during the therapy, curcumin may degrade or polymerize [16]. Therefore, the biological effects of the therapies would not be a direct result of curcumin cellular action, but rather of the products of its reactivity [16, 17]. The constantly increasing number of applications of the curcuminoid, raise the need to characterize its reactivity under various external environment conditions used in experiments to improve their therapeutic effects.

Currently, drugs characterized by low bioavailability are clinically introduced into a cancerous tissue in various ways [18]. Membrane poration techniques, like sonoporation or electroporation (EP), induce the formation of water pores in the cell membranes. When the formation of the pore is combined with the administration of the drug to the tumor site, the process is called electrochemotherapy (ECT). It is utilized to enhance the concentration of the cell-non-permeant drugs (like bleomycin or cisplatin) in the cancer tissue [19]. The increased plasma membrane permeability allows the drug to flow into the cytoplasm and exert the anticancer activity [20]. Electroporation is a technique used in superficial skin tumors as well as deeper tissues. ECT includes the coverage of melanoma lesion with the safety margin by the electrode, thus providing excellent response rate to the therapy. Nowadays, ECT is a part of different guidelines of treatment. For instance, ECT was listed in the international guidelines for skin cancer both primary and metastatic [21]. Moreover, the progress in technical development led to the use of ECT in the treatment of deep-seated tumors, like prostate cancer or bone metastases [22,23]. Study conducted by Mali et al. in 2012 showed the higher effectiveness of bleomycin/cisplatin ECT in sarcomas in comparison to carcinomas (including melanomas) [24]. In the future, several other cancer sites, like brain or lung are planned to be treated with electrochemotherapy [23]. From the technical aspect, the procedure involves only hydrophilic chemotherapeutic molecules, thus ECT with amphipathic curcumin is not a proper therapeutic choice [25]. Although curcumin is amphipathic, the products of degradation of curcumin – vanillin, ferruloylmethane, acetone and ferulic acid are the hydrophilic compounds, therefore the combination of PDT with ECT could be characterized by some anticancer potential [26, 27, 28, 29].

Curcumin has never been clinically subjected for melanoma treatment. However, the compound is currently under phase 1 of clinical trials (NCT03980509) for invasive breast cancer primary tumors treatment. Although the results are still not available, already completed clinical trial (NCT03211104) has proven that orally administered curcumin decreased the PSA levels among patients with prostate cancer [30]. In the past, both PDT and ECT underwent clinical trials. Calcium electroporation has been successfully used for treatment of cutaneous metastases of melanoma in double blinded randomized controlled phase 2 trial (NCT03628417) [31]. Currently, ECT with Pembrolizumab for superficial and visceral melanoma metastases treatment is being examined in second phase of clinical trials (NCT03448666). Conversely, photodynamic therapy was mostly subjected for choroid melanoma treatment in phase

2 (NCT01251978) and 4 (NCT01253759) of clinical trials. Moreover, skin III/IV stage melanoma was treated with verteporfin-PDT protocol (NCT00007969).

Several factors need to be considered when combining curcumin aided PDT with ECT. First, the interactions of curcumin and its degradation derivatives with the cellular membranes need to be analyzed. Subsequently, it is crucial to understand how the drug shifts from the cell membrane to the intracellular compartment, where it exhibits its anticancer activity. Another factor is the time dependence of the absorption process, namely determining the peak drug concentration in the cell and tracking its localization in time. Further studies have to include the comparison of the therapy's efficiency among different melanoma types and non-cancerous cells. The comprehensive description of the absorption process and reactivity of the drug, combined with the biological cytotoxicity assessment, would give a holistic view on the combination of ECT with PDT. Standard ECT is applied to enhance intracellular drug transportation; however, its efficacy it limited with regard to amphipathic molecules [32]. The molecular dynamics simulations of membrane-curcumin interactions revealed that curcumin localizes within the outer layer of the plasma membrane [3]. Thus due to the communication between both leaflets of the membrane, electroporation would induce an equal distribution of curcumin between both leaflets or lead to the curcumin release from the membrane [3, 30]. Besides, when curcumin flows into the cell without application of ECT, it would also bind to the membranous organelles. Therefore, the therapeutic aspect of releasing the biologically active compounds from the cellular membranes has to be verified as well. Combining ECT with PDT could induce the curcumin inflow to the cell and afterwards, the release of vanillin, feruloylmethane and ferulic acid to the cytoplasm from the membrane-water interphase [25].

This study aimed to establish the most effective protocol for the combination of curcumin-aided ECT with PDT. Four protocols, considering all the possible combinations of the therapies, have been proposed and further examined. The most effective and selective protocol was indicated and based on experiments and data presented by others authors. Four mechanisms of action were proposed, based on the applied protocol.

2. Materials and Methods

2.1 Mass spectrometry (MS) studies

MS experiments were performed on a Compact™ mass spectrometer (Bruker Daltonics, Bremen, Germany) equipped with a standard ESI source. The instrument was operated in the negative-ion mode and calibrated with the Na Formate Clusters in the HPC Calibration Mode. Spectra were recorded for samples dissolved in H_2O. Analyte solutions (200 µl) were introduced at a flow rate of 180 µl/h. The instrument parameters were as follows: scan range: 80–1300 m/z, drying gas: nitrogen, flow rate: 4.0 L/min, temperature: 180 °C and potential between the spray needle and the orifice: 4.5 kV. For MS spectra analysis, a Bruker Compass DataAnalysis 4.2 software was used. The experiments were performed in replicates and the mass spectrum with the most prominent signals from the curcumin degradation products was presented in the paper.

2.2 Molecular dynamics simulations

The experiments of curcumin localization with respect to membrane model involved the insertion of curcumin inside and outside the membrane and observation of the most stable position in which it localizes in the course of simulation. The molecular dynamics simulations were performed with GROMACS 2018.3 software [34] on the calculational cluster in the Department of Theoretical Chemistry and Physics at the Lorraine University. The models for simulations were built with CHARMM-GUI web software and visually inspected with VMD software. The simulated systems were composed of a model of the membrane and curcumin or curcumin degradation products. Simulated molecules were: vanillin, feruloylmethane, ferulic acid and acetone. The chosen molecules were grouped by the degradation

reaction pathways from the curcumin reactivity studies [16][17]. The membrane was composed of 64 lipids (70% POPC, 30% Cholesterol) per membrane layer. Before the simulation, the system was solvated in physiological conditions of NaCl water (TIP3) solution. The parameters for small compounds were obtained from CGenFF internet software. The simulation proceeded with the CHARMM36 force field. The systems were minimized, equilibrated (100 ns, NPT conditions: Nose-Hoover thermostat and Berendsen barostat) and simulated for 10 ns to inspect the localization of the examined compounds with respect to the membrane.

2.3 Cell culture

The A375 – melanotic melanoma cell line derived from the skin tissue of a 53-year-old male Caucasian patient (ATCC, London, UK). The C32 – amelanotic melanoma cell line was obtained from the skin of a 54-year-old female patient (ATCC, London, UK). Human gingival fibroblasts (HGF) were collected from the healthy patient of the Wroclaw Medical University and were used to establish the primary cell culture (HGF – patent from Saczko et al. 2008 [33]). Cells were grown in monolayer cultured in Dulbecco's modified Eagle's medium (DMEM, Sigma-Aldrich, St. Louis, MO, USA) supplemented with 10% fetal bovine serum (FBS, Sigma-Aldrich) and 1% of antibiotics solution (10 000 units penicillin and 10 mg streptomycin/mL, Sigma-Aldrich) under standard culture conditions at 37ºC in a humidified atmosphere containing 5% CO_2. When needed, the cells were rinsed with Phosphate-buffered saline (PBS, Sigma-Aldrich) and removed by trypsinization (0.025% trypsin and 0.02% EDTA; Sigma-Aldrich).

2.4 Curcumin solution preparation

The curcumin (1E, 6E)-1,7-bis-(4-hydroxy-3-methoxyphenyl)-1,6-heptadiene-3,5-dione (Sigma-Aldrich) was dissolved in dimethyl sulfoxide (DMSO, Sigma-Aldrich) to prepare 5 mM stock of the drug. Subsequently, the proper amount of stock was mixed with DMEM or EP buffer to achieve the required concentration of the drug.

2.5 Fluorescence microscopy studies of simultaneous curcumin uptake

Fluorescence microscopy was used to visualize the curcumin content in the HGF, A375 and C32 cells. The cells were incubated on cover glasses in Petri dishes overnight. Afterwards, the cells were washed 3 times with PBS and further incubated with the medium containing curcumin. After the appropriate time of incubation (0 h, 1.5 h, 3 h and 4.5 h) the medium was taken off, and the cells were fixed in 10% formalin. Afterwards, the samples were observed under the Olympus BX53F2 microscope (Olympus, Tokyo, Japan). Due to the fluorescence properties of curcumin (ex. 467 nm / em. 571 nm [34]), the content of the drug was observed after blue laser excitation (488 nm, Olympus) [34]. Samples without curcumin were used as the control and calibrants. Plan-Apochromat 20× (Olympus) objective was used to capture the images. At least 4 samples were analyzed and over 6 cells were used for curcumin content quantification of each sample. Fluorescence intensity was quantified with Fiji package of ImageJ 1.52p software (ROI Manager, Multi Measure) [35] and the statistical analysis (ANOVA) was performed with GraphPad Prism version 8.0.0 for Windows, GraphPad Software (San Diego, California USA). The differences between the fluorescence of the samples were plotted on the graphs.

2.6 Curcumin localization with respect to cellular membranes - fluorescence staining studies

CellMask Deep Red staining was performed to visualize the distribution of curcumin in the HGF, A375, and C32 cells with respect to the cellular membranes either immediately after or 3 h after the therapy. The cells were incubated on cover glasses in Petri dishes overnight to attach and then the 3 h incubation with curcumin was performed. 15 minutes incubation with CellMask Deep Red (1:1000; Thermo Fisher, C10046) was performed in parallel to end simultaneously with curcumin incubation. Afterwards, cells were fixed in 4% formalin solution. Fluorshield™ with DAPI (4,6-diamidino-2-phenylindole) was applied to visualize the nuclei and to mount the cells. The samples were observed on the Olympus FluoView FV1000 confocal laser scanning microscope (Olympus, Tokyo, Japan).

2.7 Membrane permeabilization in response to pulsed electric field (PEF) – flow cytometry studies

The efficiency of cell membrane permeability in response to the electric field among malignant (A375) and normal (HGF) cells was analyzed by flow cytometry (Cube-6, SYSMEX EUROPE GmbH, Warsaw, Poland). Cells were harvested on 6-well plates in the number of 2×10^5 cells per well. The cells were detached with trypsin, centrifuged and suspended in electroporation phosphate buffer (Na_2HPO_4/NaH_2PO_4, $MgCl_2$, sucrose). Cells were maintained in suspension and pulsed in a cuvette (VWR) with two aluminum plate electrodes (2 mm gap). Afterwards, the cells were treated with 200 to 1400 V/cm PEFs with 200 V/cm step (8 pulses, 10 Hz, 100 μs). The applied protocol was previously optimized for the cell culture. Then, the cells were incubated for 10 minutes at 37◦C in a humidified atmosphere containing 5% CO_2. In the next step, cells were washed in PBS, centrifugated and resuspended in 0.5 mL of PBS. Flow cytometry analysis was performed using a Cube 6 flow cytometer (Sysmex, Warsaw, Poland). The fluorescence of PI was excited with 488 nm laser and assessed with the FL-3 detector (700/50). Data was collected and analyzed by CyView software (Sysmex, Warsaw, Poland).

2.8 Drug uptake in response to ECT – flow cytometry studies

The efficiency of curcumin absorption in response to the electric field in malignant (A375) and normal (HGF) cells was analyzed by flow cytometry. Cells were harvested on 6-well plates in the number of 2×10^5 cells per well. The cells were detached with trypsin and harvested in electroporation phosphate buffer (Na_2HPO_4/NaH_2PO_4, $MgCl_2$, sucrose). Cells were maintained in suspension and pulsed in a cuvette (VWR) with two aluminum plate electrodes (2 mm gap). Before the EP protocol, curcumin was added to the cell suspension to a final concentration of 7 μM. Afterwards, the cells were treated with PEFs varying from 100 to 1400 V/cm (step 100 V/cm, 8 pulses, 10 Hz, 100 μs). The applied protocol was previously optimized for the cell culture. Then, the cells were incubated for 10 minutes at 37°C. In the next step, cells were washed in PBS, centrifugated and resuspended in 0.5 mL of PBS. Flow cytometry analysis was performed using a Cube 6 flow cytometer (Sysmex, Warsaw, Poland). The fluorescence of cells loaded with curcumin was assessed with FL-2 detector (580/30). Normalized median fluorescence was calculated as the difference between the fluorescence of electroporated sample with curcumin and fluorescence of electroporated sample without curcumin.

2.9 PDT experiment

PDT was performed with the polarized light lamp (Optel, Poland). The radiation power density was set to 20 mW/cm^2. The peak of curcumin light absorption (410 nm) matches the wavelengths represented by the blue light, lamp with the blue-polarized filter was used to perform the photodynamic reaction [9]. Before each experiment, the irradiance homogeneity, as well as the light power, was tested using a radiometer (MRT-06, Optel, Poland). For all tested protocols PDT parameters were the same. Cells were seeded in 96-well plates in the count of 2×10^4 (A375, C32) or 4×10^4 (HGF) cells per well and incubated overnight in complete growth medium to allow for cell attachment. Then DMEM was replaced with media containing 10 μM of the photosensitizer. Some of the samples were irradiated simultaneously and the others after the 3 h incubation time. Subsequently, the culture medium, containing the drug, was replaced with curcumin-free DMEM. The cell mitochondrial metabolic activity measurements (MTT) were carried out after 48 hours of incubation in the CO_2 incubator.

2.10 ECT experiment

EP was performed with the ECM 830 electroporator (BTX, Syngen Biotech, Poland, Wroclaw and Petri pulser plate electrode with 2 mm distance between the electrodes (FID GmbH, Germany). Electric fields ranging from 0 to 1200 V/cm were applied in the flow cytometry experiments. Electric fields 0, 600 and 1200 V/cm were used in the mitochondrial metabolic activity assay. 1200 V/cm was used in all of the combinational therapies experiments. Each experiment involved the application of 8 pulses with 10 Hz frequency and 100 μs pulse duration. Before each

experiment, the apparatus was calibrated to provide the exact electric field. The generated electric fields varied less than 5% from the set value, which was confirmed using an oscilloscope during each experiment.

For the viability experiments, the HGF, A375 and C32 cells in the number of 2×10^5 cells per well were seeded in 6-well plates (Thermo Fisher). The cells were incubated overnight in complete growth medium to allow the cells to attach. Then the medium was replaced with the electroporation buffer (10 mM phosphate buffer pH=7.4, 1 mM $MgCl_2$ and 250 mM sucrose) with 10 µM final curcumin concentration. First group of samples was treated with PEFs in the first 10 s after curcumin's addition. The other group of samples underwent the 3 h incubation time in DMEM with 10 µM curcumin, after which the medium was replaced with curcumin-free electroporation phosphate buffer and eventually electroporated. After electrochemotherapy, the electroporation buffer was exchanged with curcumin-free culture medium (DMEM). The mitochondrial activity assay (MTT) was carried after 48 h of incubation.

2.11 Combination of ECT with PDT experiments

HGF, A375 and C32 cells were seeded on the 6-well cell culture plates in the number of 2×10^5 cells per well. Before the experiment, the cells were incubated overnight in complete growth medium to allow for cell attachment. Four protocols were established for the experiments (Schematic 1).

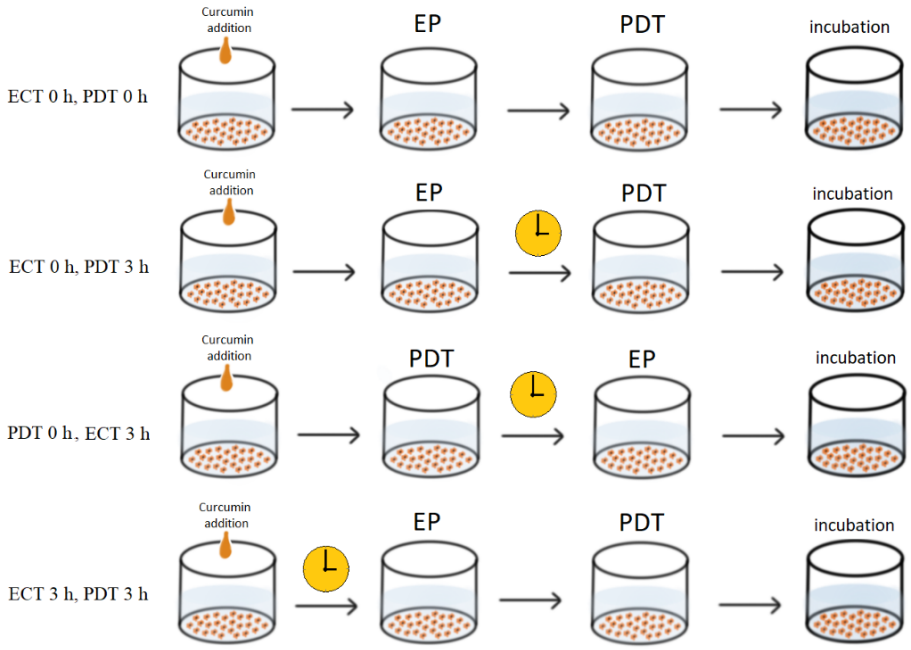

Schematic 1. Investigated therapies – simplified scheme; orange droplet shows the addition of curcumin, clock indicates the 3 h incubation time, arrows – the instant procedure; after all the experiments, the cells were left for 48 h incubation and the biological effects were assessed afterwards.

1. "ECT 0 h, PDT 0 h" – the culture medium was replaced with the ECT buffer containing 10 µM curcumin, further the cells were instantly electroporated and afterwards, the buffer was replaced with the curcumin-free medium. In the end, the cells were irradiated. This protocol is the most intuitive, and thus, most other authors use it as standard in their research [29]. The approach included negligible metabolism of the drug, leading to a higher concentration of the photosensitizer in carcinoma cells.

2. “ECT 0 h, PDT 3 h” – the culture medium was replaced with the ECT buffer with 10 μM curcumin, further the cells were instantly electroporated and afterwards incubated for 3 h in the curcumin-free medium. Next, the cells were irradiated with the blue light. The purpose of the 3 h incubation was to enable the intracellular distribution of curcumin within the membranous organelles prior to irradiation.

3. “PDT 0 h, ECT 3 h” – the culture medium was diluted to obtain 10 μM curcumin concentration, further the cells were instantly irradiated and afterwards incubated for 3 h in the medium. After incubation, the medium was replaced with the curcumin-free ECT buffer, and the samples were electroporated. In the end, the buffer was replaced with DMEM. This approach aimed to investigate the effect of curcumin reactivity products on the efficiency of ECT.

4. “ECT 3 h, PDT 3 h” – the culture medium was diluted to obtain 10 μM curcumin concentration, further the cells were incubated for 3 h. Following incubation, the medium was replaced with the curcumin-free ECT buffer, and the samples were electroporated. The ECT buffer was further replaced with DMEM and the samples were irradiated. This approach remains similar to the first one, however, the difference lies in the cellular distribution of curcumin. After 3 h of incubation, the drug is mainly localized in the intracellular membranes whilst in the first option curcumin surrounds the plasma membrane.

The control without curcumin underwent the same media changes to eliminate the uncontrolled loss of cells. After 48 h incubation following the experiments, the mitochondrial metabolic activity of the cells was assessed with MTT assay, alkaline comet assay and caspase-12 staining studies.

2.12 MTT cell viability assay

To perform the MTT assay, the culture medium was removed from the wells, and 100 μl of 0.5 mg/ml MTT (3-(4,5-dimethylthiazol-2-yl)-2,5-diphenyltetrazolium bromide, Sigma) solution in PBS buffer was added to the 96-well plates; for the 6-well plates, the volume of MTT reagent was 0.5 ml. After 2 h incubation at 37˚C, acidified isopropanol (100 μl, 0.04 M HCl in 99.9% isopropanol) was added to dissolve the formazan crystals. The absorbance of each well was measured at 570 nm using the multiplate reader (Promega, GmbH, Germany). The results were normalized to control (100%) and plotted.

2.13 Caspase-12 immunofluorescence staining studies

Confocal laser scanning microscopy was applied to assess the caspase-12 expression and distribution in the HGF, A375 and C32 cells after the combinational therapies. Caspase-12 was used to evaluate the endoplasmic reticulum associated apoptosis. The cells were incubated on cover glasses in Petri dishes overnight. Above the described combinational therapies experiments were performed afterwards. After 48 h of incubation, the cells were washed 3 times with PBS. The cells were fixed in formalin and incubated with the first order anti-caspase-12 rabbit antibody (1:100; Santa Cruz, sc-5627) for 1 h in the 37ºC incubator in a humidified atmosphere. Following the incubation, the cells were washed in PBS. Afterwards, the secondary anti-rabbit antibody conjugated with Alexa Fluor-488 (4 μg/ml; Invitrogen, A11008) was added and left for 2 h incubation in 37˚C. Fluorshield^{TM} with DAPI (4,6-diamidino-2-phenylindole) was applied to visualize the nuclei and to mount the cells. The samples were observed on the Olympus FluoView FV3000 confocal laser scanning microscope (Olympus, Tokyo, Japan). Plan-Apochromat 60× oil immersion objective (Olympus) was used to capture the images. To analyze the total content of caspase-12 in the cell, photographs proceeded as the z-stacks, rather than the single plane captures. Microscopy photographs were analyzed with FIJI [36].

2.14 Alkaline comet assay

Alkaline comet assay method described by Collins, 2002 [37]. was used for detection of DNA damages after the previously described combinational therapies. Slides were submerged in precooled lytic solution (100 mM EDTA, 2.5 M NaCl, 10 mM Tris, and 1% Triton X-100, pH 10) at 4°C for 60 min. After lysis, slides were equilibrated in electrophoretic solution (300 mM NaOH, 1 mM EDTA, pH > 13) for 30 min, after that electrophorese was set at 1.2 V/cm for 30 min. Finally, the slides were washed in neutralization buffer (0.4 M Tris, pH 7.5). For scoring the comet patterns, > 50 nuclei from each slide were assessed. Besides, the samples were stained using fluorescent dye Propidium Iodine. The images were acquired on a fluorescent microscope (Olympus BX53F2, Japan). The CometScore 2.0 software was used to analyze the comets. The percentage of DNA in the comet tail was taken as a quantified index of DNA damage. To visualize the relative number of cells with extensive (> 40%) and lesser DNA fragmentation (15-40%), the cells were counted and presented on the cumulative graphs. Similar attempt was used by Cortés-Gutiérrez et al. [38].

2.15 Statistical analysis

The experiments were performed in replicates. Data were expressed as mean ± SD and were analyzed by ANOVA coupled with multiple comparison technique - Tukey's test (in GraphPad Prism 8), with $p<0.05$ being considered statistically significant (ns – not significant). Statistical analysis was incorporated to the graphs – when two groups of were compared, the statistic lines directly connected both of them. When the same statistical result related to the whole set of results, there was presented a single statistic line / point above the particular results.

3. Results

3.1 Mass spectrometry studies

Mass spectrometry was used to determine the stability of curcumin after application of external electric field and light. Comparison of the curcumin mass spectra before and after the irradiation, revealed the decreased peak in 367.11 m/z, which indicates, the diminish in curcumin content. However, additional peaks in 121.03, 151.04, 193.05 m/z were observed. The peaks are associated with the occurrence of new molecules in the solution – vanillin, ferulic acid and ferruloylmethane, respectively (Figure 1). Additional peaks of curcumin were observed in the spectra as well, however these were a result of the compounds decomposition during the measurements. Between various replicates, the ratio between curcumin and curcumin degradation products differed, however, in each case, after irradiation of curcumin, the same additional peaks occurred.

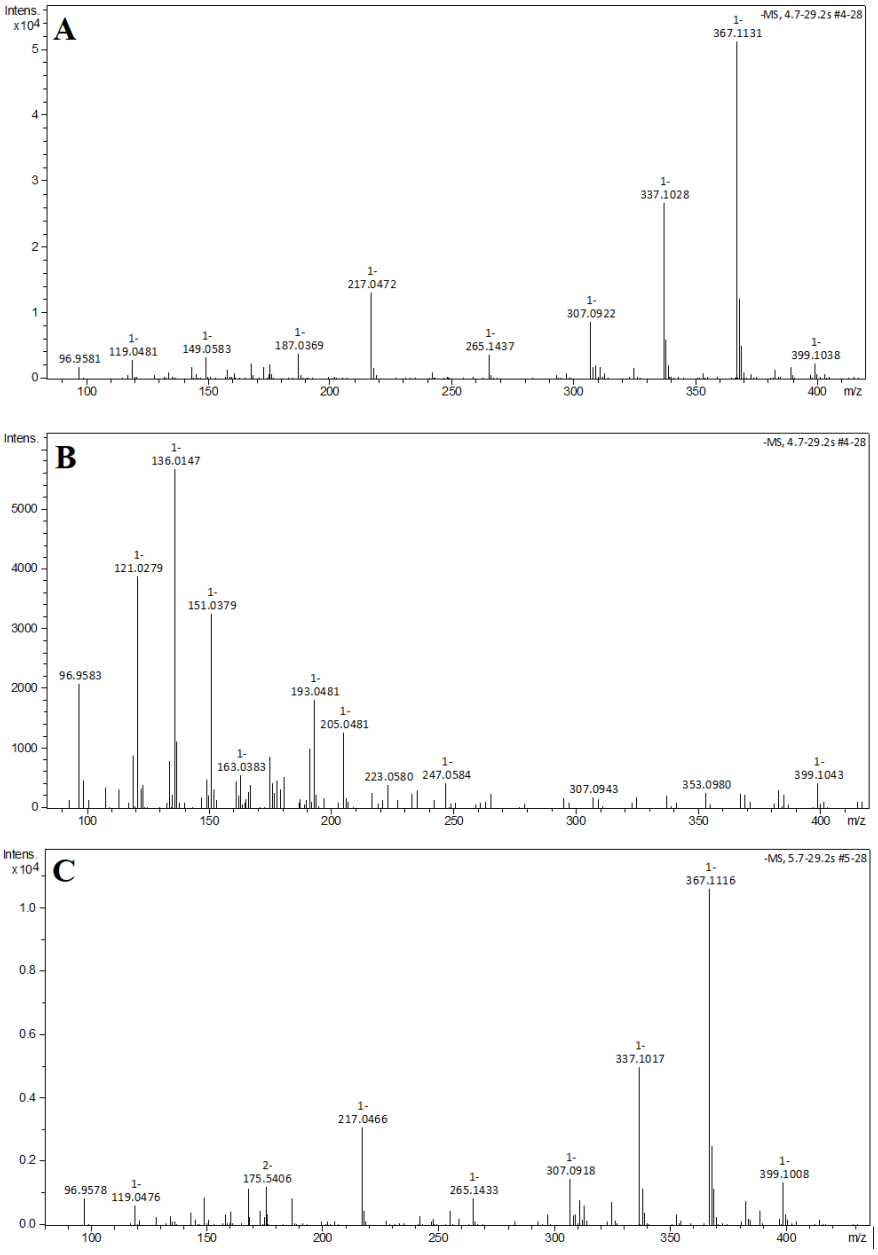

Figure 1. Mass spectrometry spectra of curcumin (A); curcumin after irradiation for 3 minutes with 20 mW/cm^2, 420 nm light source (B); curcumin after application of electric field (1.2 kV/cm, 8 pulses, 100 µs duration) (C);

The analysis of curcumin spectra after application of the electric pulses (1.2 kV/cm, 8 pulses, 100 µs duration) did not lead to any structural changes. The signal intensity differed; however, no additional peaks were observed in the MS spectra. The thesis about formation of curcumin multimers was rejected due to the lack of higher mass compounds.

3.2 Curcumin and degradation products localization with respect to cellular membranes – molecular dynamics studies

Molecular modelling is with an agreement with other researchers' theses that curcumin localizes in the membrane-water interface due to its amphipathic properties [3]. The hydrophilic hydroxide groups protruded into the solution,

and the hydrophobic aromatic rings stayed stable in the hydrophobic core of the membrane. Curiously, only one of two feruloylmethane groups remained in the membrane. Therefore, curcumin was connected with the leaflet of the membrane, to which it initially adhered and it did not communicate with the other leaflet. The systems were simulated under NPT conditions, which enabled the expansion of the membrane in xy-plane due to the insertion of the drug. With the increasing membrane size, the "area-per-lipid" value increased.

Presented molecular dynamics experiments (Figure 2) show the extramembrane localization of the hydrophilic products of the curcumin's degradation. The compounds were released from the membrane to the water solution. Except from acetone (Fig. 2D), none of the curcumin derivatives exhibited interactions with the surface of the membrane. The small molecule compounds were released from the membrane in the process of system equilibration and the proper simulation afterwards did not lead to any ligand-membrane interactions. Curcumin degradation products are hydrophilic in contrast to the initial compound. Moreover, the small molecules lack in the long conjugated π-bonds system.

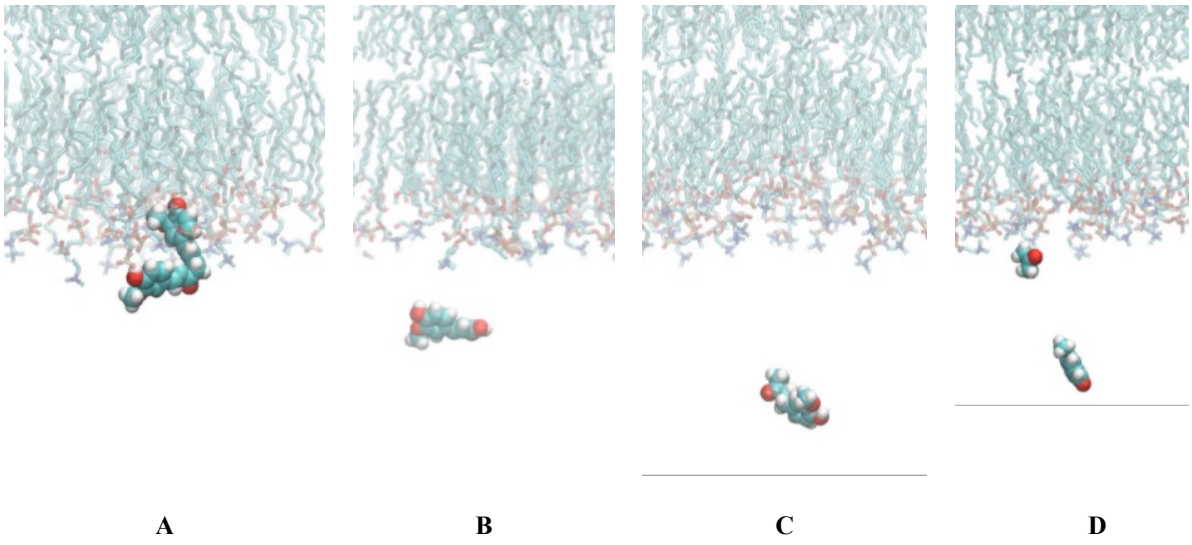

Figure 2. Molecular dynamics approach for visualization of interactions of A) Curcumin, B) Ferulic acid, C) Feruloylmethane, D) Vanillin and acetone with the membrane model (70% POPC, 30% Cholesterol)

3.3 Curcumin uptake – fluorescence microscopy studies

The fluorescence studies aimed to establish the profile of curcumin's absorption in time (Figure 3).

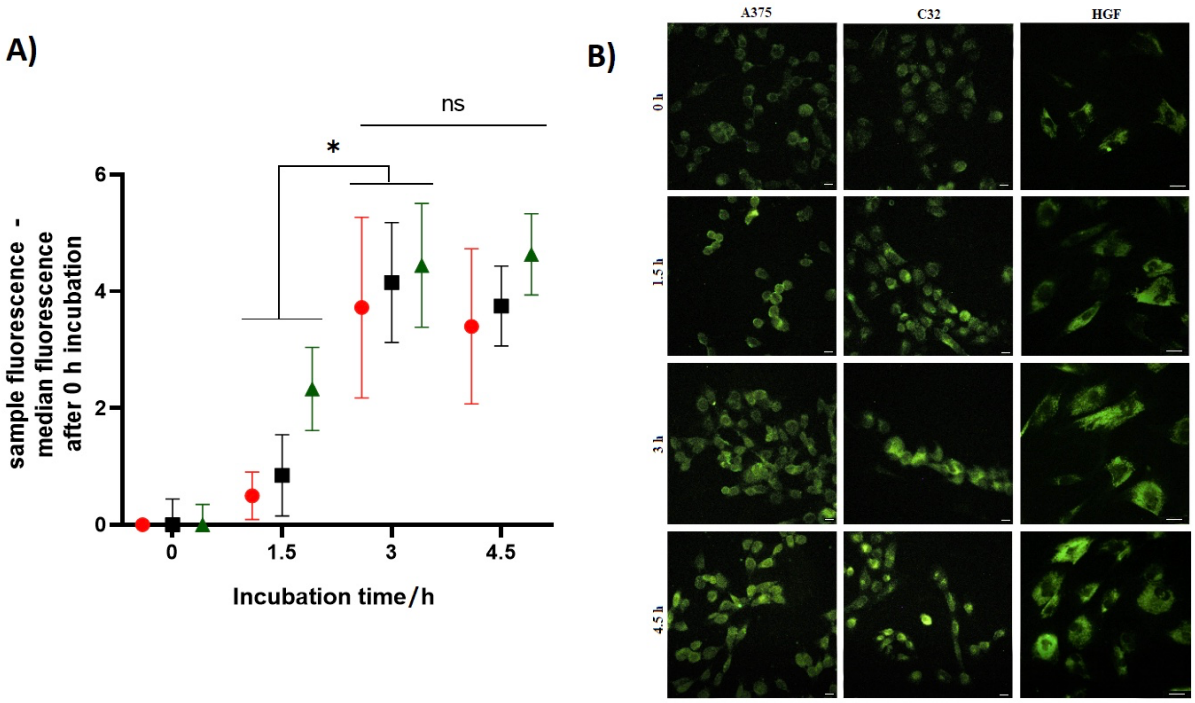

Figure 3 Curcumin uptake in time: A) statistical analysis (different color of spots indicate the uptake of curcumin by HGF cells - red, A375 cells - black and C32 cells - green) and B) fluorescence microscopy samples of HGF, A375 and C32 cells after 0, 1.5, 3 and 4.5 h incubation with 10μM curcumin; Scale bar = 10 μM; two-way ANOVA * $p<0.005$, ns $p>0.9$ ($N \geq 24$); when the statistical analysis related to the whole set of results and was presented a single statistic line above them.

The statistical analysis of the results revealed that after 3 h of incubation, the drug reaches the maximum cellular level and there are no differences in comparison to longer incubation time (like 4.5 h). Thus, for further studies, the two most interesting incubation times were selected – 0 h and 3 h. The plot shows different curcumin absorption rate as well. C32 cells absorb the drug more rapidly in comparison to the others. After 1.5 h, HGF and A375 cell's absorption remained at the same level. Standard deviation of absorption of curcumin increased with the incubation time as well, showing the difference in long-term absorption rate between cells in various physiological conditions, such as division or apoptosis.

3.4 Simultaneous curcumin cellular localization with respect to cellular membranes

As demonstrated in Figure 4, aside from the nucleus, curcumin is distributed evenly within the cell right after its application. However, after 3 h of incubation the fluorescence signal concentrates in intracellular membranes. The intensity of the signal highly progressed over incubation time. The tendency was observed in melanotic (A375) melanoma and amelanotic (C32) melanoma cells. Although the distribution of curcumin among fibroblasts was not even starting from the 0 h incubation time, fluorescence signal intensity progressed. The difference between malignant and normal cells was observed in the distribution of curcumin just after addition.

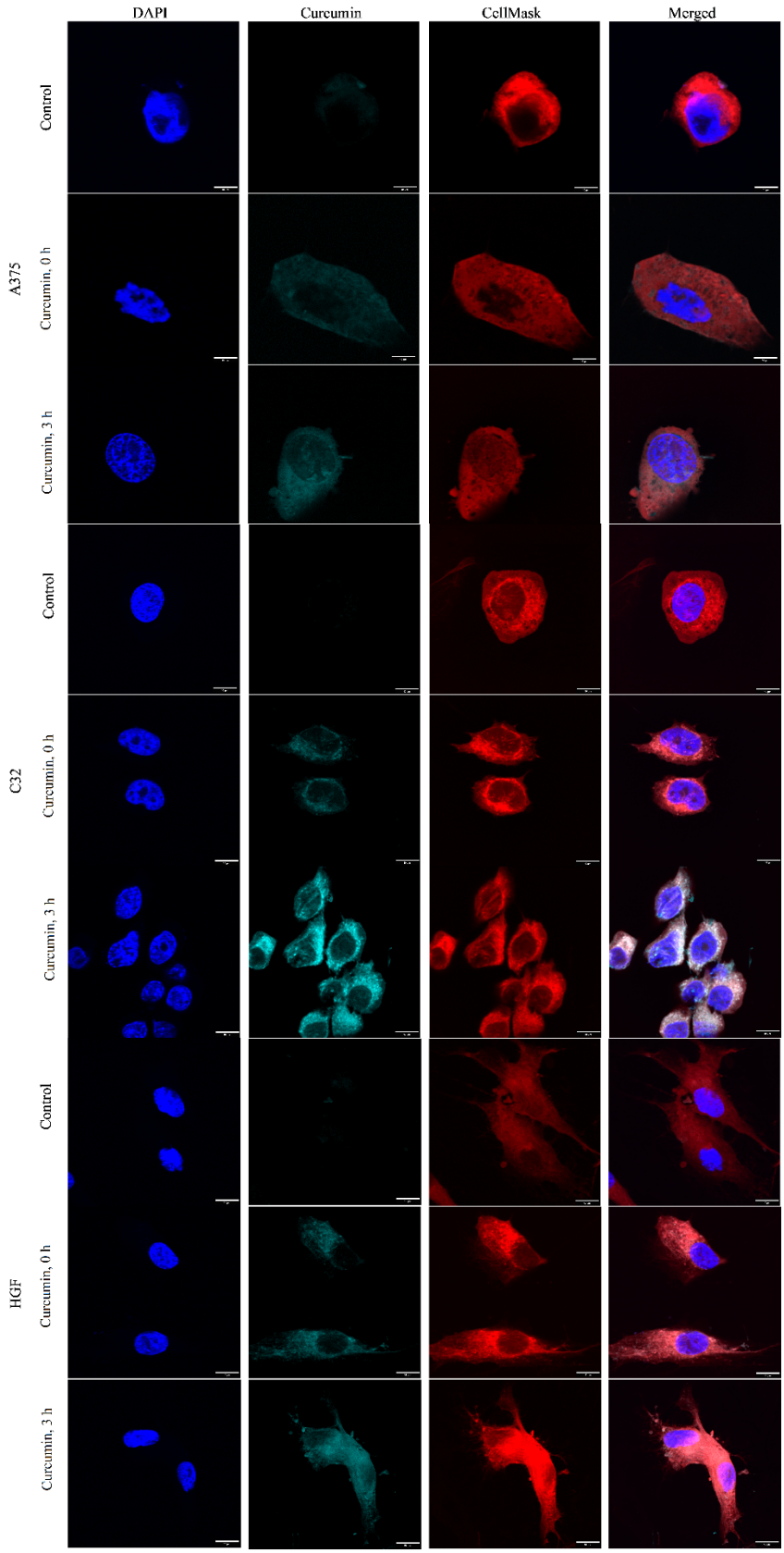
DAPI
Curcumin
CellMask
Merged
A375
C32
HGF
Control
Curcumin, 0 h
Curcumin, 3 h
Control
Curcumin, 0 h
Curcumin, 3 h
Control
Curcumin, 0 h
Curcumin, 3 h

Figure 4. The intracellular localization of curcumin in A375, C32 and HGF cells after instant addition and removal of 10 µM curcumin solution (0 h) and after 3 h incubation with 10µM curcumin solution; Nuclei stained with DAPI and biological membranes with CellMask Deep Red; Control – cells without curcumin; Scale bar = 10 µM;

3.5 Membrane permeabilization and curcumin's cellular content after ECT

The permeability of cell membrane (Figure 5) increased with the increasing electric field. For the study were selected one melanoma cell line and normal cells to compare the effect of electric pulses. In both malignant (A375) and normal (HGF) cell lines, the permeabilization for PI was similar in each of the analyzed electric fields – ANOVA analysis revealed no statistically significant differences between the cell lines. Although the tendency remained the same, in 1.2 kV/cm electric field, the difference between both cell lines was presented by $p < 0.0001$ in the two-way ANOVA analysis. The increase in membrane permeability was observed between 600 and 800 V/cm electric fields. From 600 V/cm the increase in permeable cells develops linearly. In 1.4 kV/cm electric filed, almost all cells remain permeable. The difference between malignant and normal cells occurs only in 1200 V/cm.

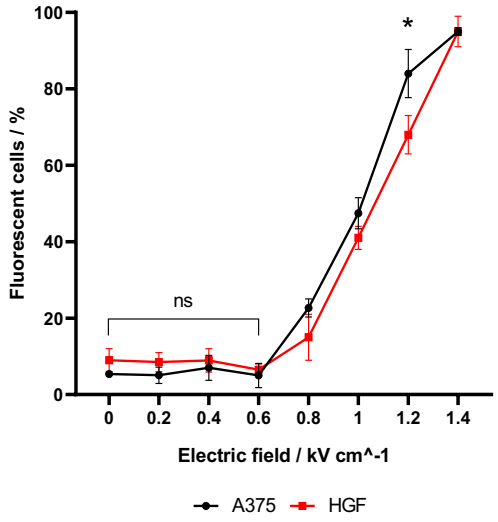

Figure 5. PI permeabilization of cell membranes of A375 and HGF cells in response to the electric field (0-1.4 kV/cm, 8 pulses, 100 µs pulse, 10 Hz); two-way ANOVA: * $p < 0.0001$, ns $p > 0.05$, N=3; the statistic lines connect two of the compared groups (in both cell lines); to present the difference between cell lines, * was inserted above the analyzed voltage parameter.

In the curcumin uptake experiments, there was observed a decrease in curcumin fluorescence with the increasing electric field in both cell lines (Figure 6). The downfall starts in relatively low electric fields – 100 V/cm decreases the curcumin content by ~10% among HGF and ~20% among A375. However, there is no statistically significant difference between the cell lines in the two-way ANOVA analysis. For further studies, 600 and 1200 V/cm electric fields were chosen.

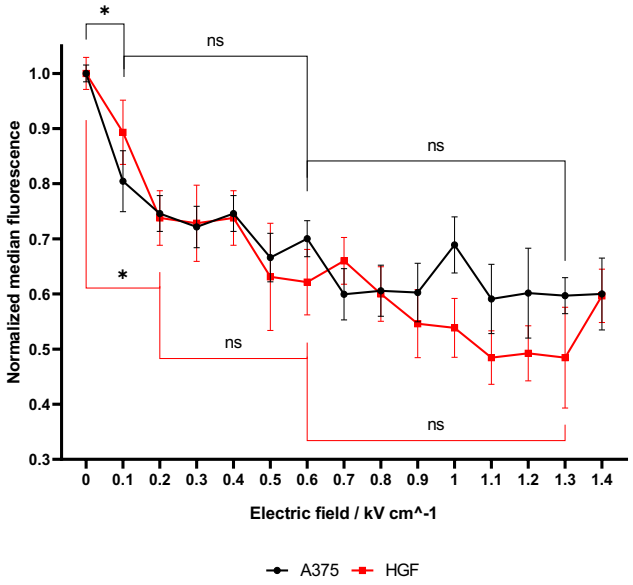

Figure 6. Curcumin fluorescence in A375 and HGF cells after electroporation (0-1.4 kV/cm, 8 pulses, 100 µs); two-way ANOVA: * $p < 0.0001$, ns $p > 0.05$, N=3; the statistic lines connect two of the compared groups.

3.6 MTT viability assay

Figure 7 demonstrates that cells are more susceptible to irradiation instantly after the addition of 10 µM curcumin in comparison to the 3 h of incubation forwarded by irradiation. Medium replacement was done to evaluate if the incubation with degradation products of curcumin leads to the higher decrease in mitochondrial activity in comparison to incubation with curcumin. Both A375 and HGF cell lines presented the same tendency – there were no statistical differences between the cells that underwent the medium replacement and the cells without media replacement after irradiation. In case of C32 cell line, there was observed higher cytotoxic effect, when there was no medium replacement. The toxicity of the therapy was significantly higher when the PDT was applied immediately after curcumin addition compared to PDT preceded by 3-hour incubation with curcumin. Generally, HGF cell line was significantly more resistant to the therapy than both A375 and C32 melanoma cell lines ($p < 0.0001$).

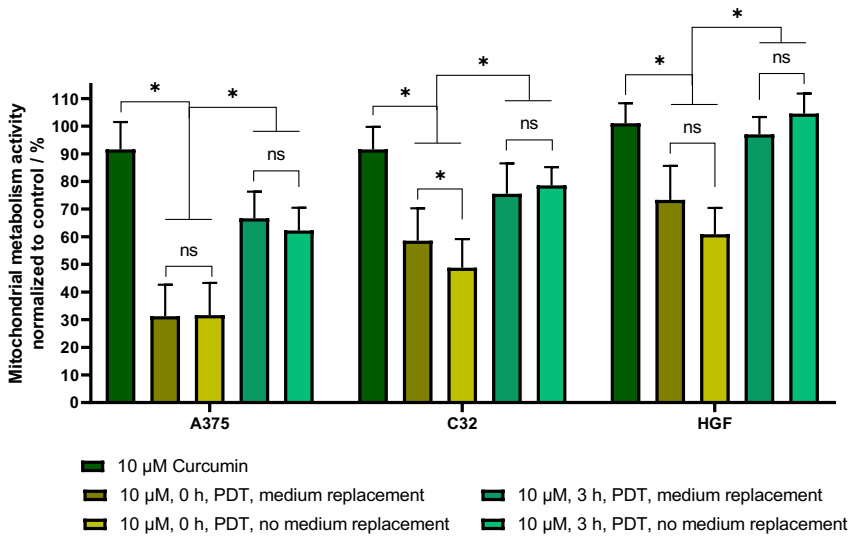

Figure 7. The results of MTT assay following cytotoxicity tests with 10 µM curcumin and 10 µM curcumin-aided PDT (420 nm, 20 mW/cm^2, 3 minutes irradiation time) on HGF, A375 and C32 cell lines after 48 h of incubation. The samples were incubated with curcumin for 0 or 3 h before PDT. Statistically significant differences between cells exposed to PDT and nontreated control (two-way ANOVA * $p<0.05$; ns $p>0.05$, $N \in <10, 25>$); the statistic lines directly connecting columns, link both compared groups; the statistic lines above the graph compare all the columns below the line with each other.

Figure 8 shows two patterns in which the cells react to the electroporation with curcumin. Among C32 and HGF cells, there was observed the tendency to increase the average mitochondrial activity with the increasing time of incubation. However, the increase was not always statistically significant. The other tendency was observed among A375 cell line – the cells highly increased their mitochondrial activity in response to the simultaneous electroporation after curcumin addition. However, when the incubation time reaches 3 h, the cells did not differ from the control without the addition of the drug. The standalone effect of 1200 V/cm electric field treatment decreased the mitochondrial activity to 75.86%, 85.70% and 81.22% in A375, C32 and HGF cells respectively. Interestingly, standalone 600 V/cm treatment led to the decrease of the mitochondrial activity to almost the same level (88 ± 1.5%) in all the analyzed cell lines

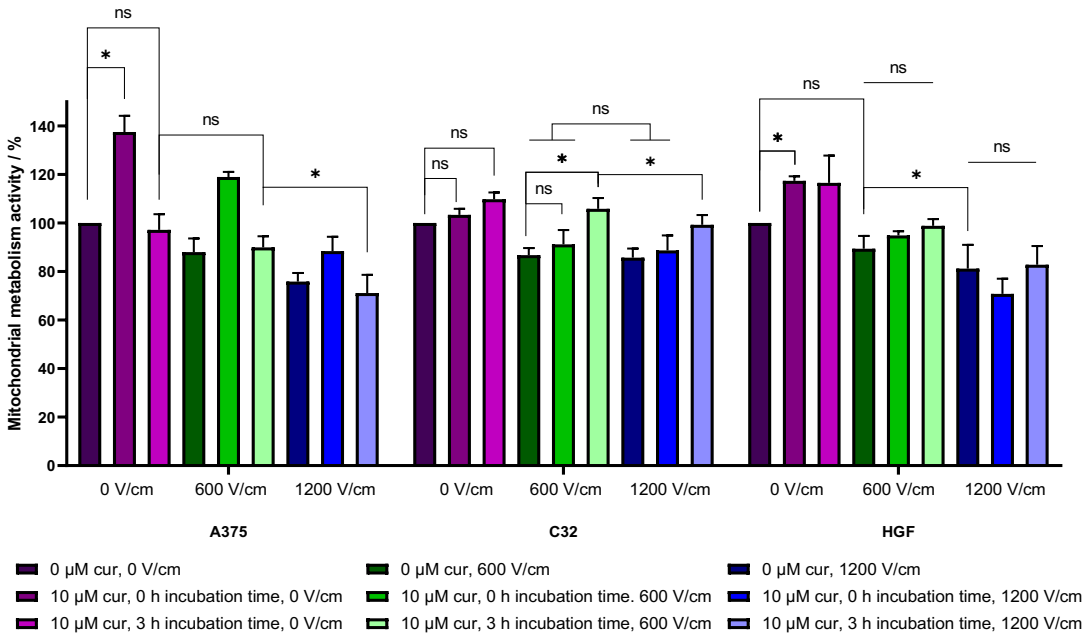

Figure 8. The results of MTT assay following cytotoxicity tests with 10 μM curcumin and 10 μM curcumin-aided ECT (0, 600 and 1200 V/cm, 8 pulses, 100 μs duration) on HGF, A375 and C32 cell lines after 48 h of incubation. The samples were incubated with curcumin for 0 or 3 h before ECT. Statistically significant differences between cells exposed to ECT and nontreated control (two-way ANOVA * $p<0.05$; ns $p>0.05$, $N \in <3, 6>$); the statistic lines directly connecting columns, link both compared groups; the statistic lines above the graph compare all the columns below the line with each other.

Figure 9 shows the especially high mitochondrial metabolism activity-decreasing properties of the "ECT 0 h, PDT 0 h" therapy. In HGF and C32 cell lines the mitochondrial activity was decreased by 97.99% and 81.69%, respectively. "ECT 0 h, PDT 3 h" induced the decrease in mitochondrial activity to nearly the same 50% level among all the analyzed cell lines. "PDT 0 h, ECT 3 h" appeared to be nearly as effective; however only towards the A375 cells. However, in this case, the results should not be directly compared to the other protocols, due to the fact that curcumin was initially dissolved in DMEM and not like in the other protocols in the electroporation buffer. "ECT 3 h, PDT 3 h" therapy was the least effective, decreasing the mitochondrial metabolism activity of each cell line to 60-70% range. Analysis with respect to cell lines showed, that A375 cells were mostly affected by the therapies involving initial PDT. Melanotic melanoma was not dependent on the timing of ECT. Conversely, C32 cells showed much higher regular dependence on time of ECT application. When the incubation time increased to 3 h, the mitochondrial activity did not confide on the timing of PDT. Among fibroblasts there has been no difference in mitochondrial activity after the therapies involving the gap between ECT and PDT. The cells were highly susceptible to the instant electrochemotherapy followed by photodynamic therapy, however the increase in incubation time led to higher mitochondrial metabolic activity. The results show that curcumin metabolic degradation extends with the increasing incubation time. Generally, C32 melanoma was the most resistant of all three analyzed cell lines ($p<0.05$).

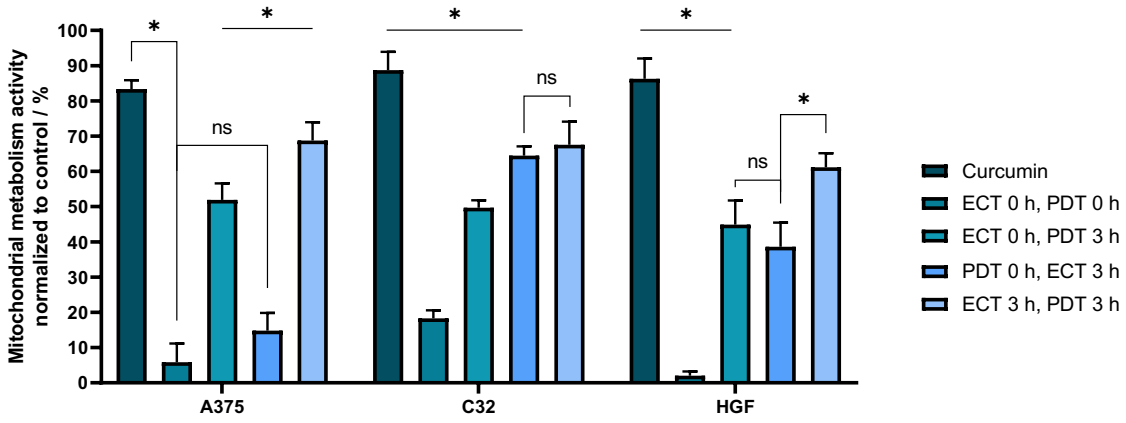

Figure 9. The results of MTT assay following cytotoxicity tests with 10 µM curcumin and combination of 10 µM curcumin-aided ECT (1.2 kV/cm, 8 pulses, 100 µs duration) with 10 µM curcumin-aided PDT (420 nm, 20 mW/cm^2, 3 minutes irradiation time) on HGF, A375 and C32 cell lines after 48 h of incubation. The samples were incubated with curcumin for 0 or 3 h before ECT and PDT. Statistically significant differences between cells exposed to ECT, PDT and nontreated control (two-way ANOVA * $p<0.05$; ns $p>0.05$, $N \in <3, 7>$)); the statistic lines directly connecting columns, link both compared groups; the statistic lines above the graph compare all the columns below the line with each other.

3.7 Caspase-12 immunostaining studies

Caspase-12 staining studies were performed to examine the induction of endoplasmic reticulum (ER) associated apoptosis in the analyzed therapies (Figure 10). Translocation from ER to the cytoplasm and further to the nucleus is crucial for exceeding the DNA-cutting activity of caspase-12. Therefore, the fluorescent regions in nuclei exhibit the active caspase-12 [39]. Both malignant and normal cell lines exhibited caspase-12 inclusion bodies (caspase-12 increased intensity regions) in the nuclei after the "ECT 0 h, PDT 0 h" therapy. In "ECT 3 h, PDT 3 h" caspase-12 in also present in the nuclei. However, the fluorescence was much lower and the morphology of the caspase-12 inclusive bodies in the nuclei was altered in C32 amelanotic melanoma cell line. Namely, the nucleus was full of caspase-12, however the protein did not form any inclusions. "PDT 0 h, ECT 3 h" therapy induced the production of caspase-12 aggregates in the A375 cells nuclei and the overload of the caspase-12 in C32 nuclei. The presence of caspase-12 inclusion bodies in the cells' nuclei correlated positively with the decrease in mitochondrial activity in MTT assay. Besides, the presence of diffused caspase-12 in the nucleus was not connected with mitochondrial activity loss, but rather with the induction of early apoptosis among the cells, showed in DNA fragmentation studies. Noteworthy, the

"ECT 3h, PDT 0 h" therapeutic approach induced the transport of caspase-12 to the nuclei but only in melanoma cells and not in human fibroblasts.

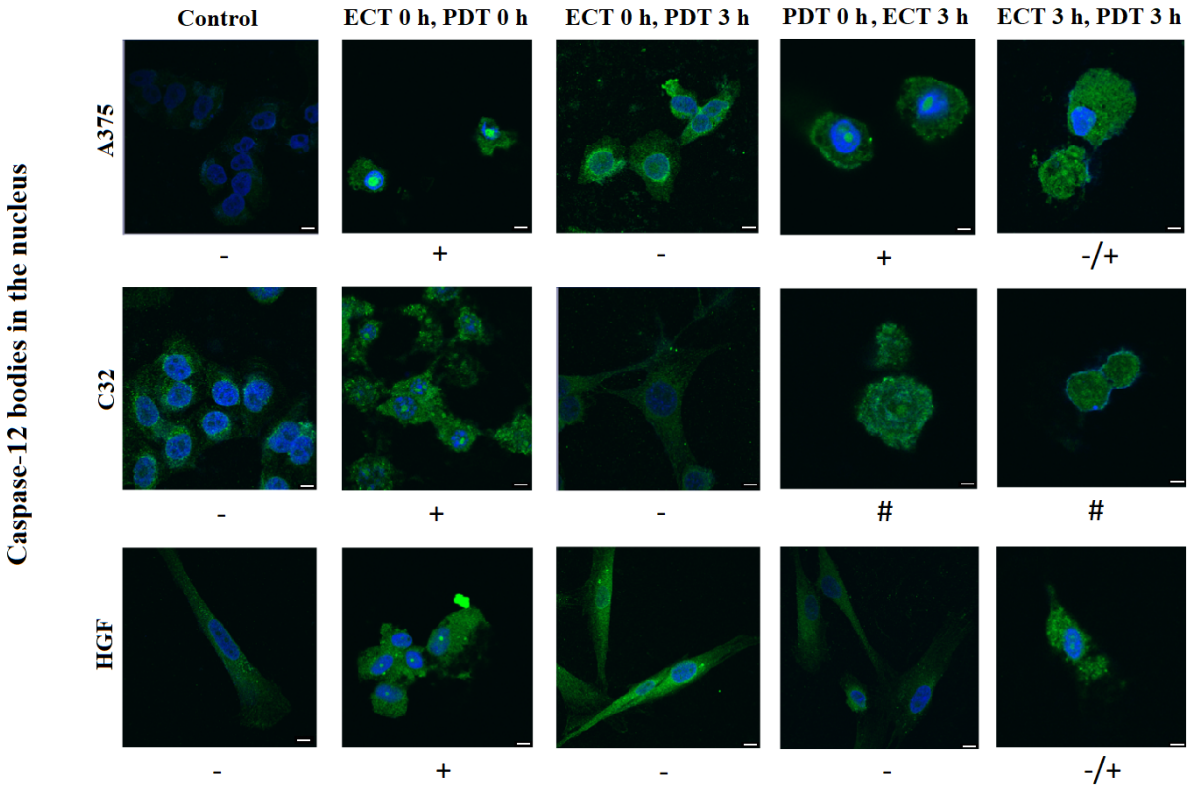

Figure 10. Caspase-12 expression among the cells after combination of 10 µM curcumin-aided ECT (0, 600 and 1200 kV/cm, 8 pulses, 100 µs duration) with 10 µM curcumin-aided PDT (420 nm, 20 mW/cm^2, 3 minutes irradiation time) on HGF, A375 and C32 cell lines after 48 h of incubation. The samples were incubated with curcumin for 0 or 3 h before ECT and PDT; Scale bar = 10 µM; Symbols below the photographs summarizes the caspase-12 bodies occurrence in the nucleus; (+ present, - absent, -/+ the intensity is lower but still present, # the nucleus morphology is changed and seems to be full of caspase)

3.8 *Comet assay*

The alkaline comet assay (Figure 11) revealed that the fragmentation of DNA varies, depending on the cell line. Fragmentation reached over 90% in the most effective A375 melanoma-targeting therapies. For instance, the „ECT 0 h, PDT 0 h" and "PDT 0 h, ECT 3 h" protocols led to the statistically significant however highly variable DNA damage across the analyzed comets. The therapies that induced the most DNA-fragmentation among C32 cells were "ECT 0 h, PDT 0 h" and "ECT 3 h, PDT 3 h". High variance between the single comets were observed in "ECT 3 h, PDT 3 h" therapy. Although in this case, the average value of tail DNA was low, significant number of cells exhibited up to 100% fragmentation levels. In contrast, the percentage of DNA in the tails of the comets did not exceed 30% among fibroblasts. The selectivity of the caspase-12 induced DNA damage was related to the smaller nuclei caspase-12 inclusion bodies in the nuclei of the fibroblasts in comparison to both melanomas. A similar case happened in A375

treated with “ECT 3 h, PDT 3 h” therapy. The cells did not exhibit the centrally situated bodies but rather diluted and smaller ones.

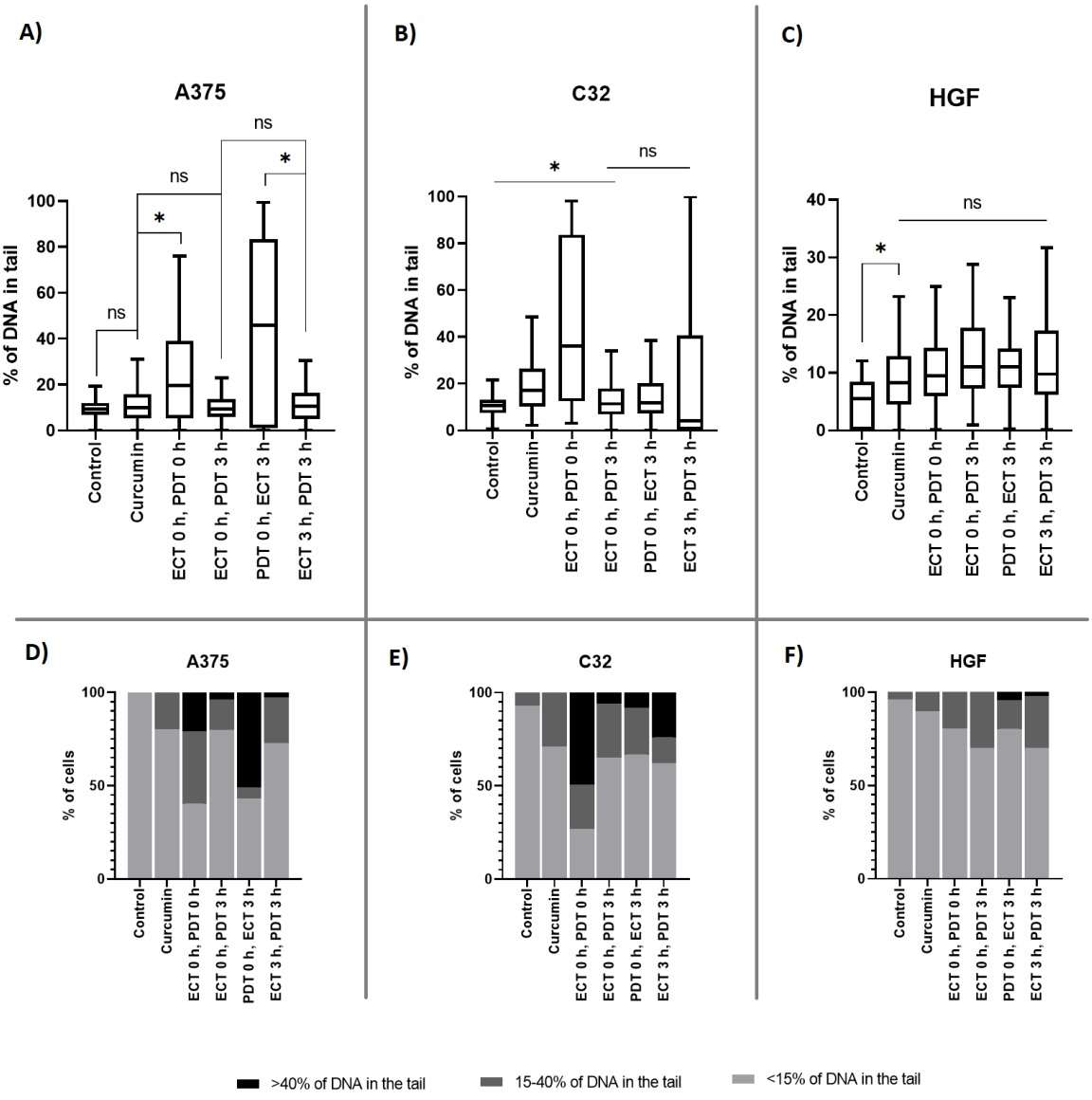

Figure 11. DNA fragmentation of A) A375, B) C32, C) HGF cells after combination of 10 µM curcumin-aided ECT (1.2 kV/cm, 8 pulses, 100 µs duration) with 10 µM curcumin-aided PDT (420 nm, 20 mW/cm^2, 3 minutes irradiation time) on HGF, A375 and C32 cell lines after 48 h of incubation. The samples were incubated with curcumin for 0 or 3 h before ECT and PDT.; * $p<0.0001$, ns $p>0.05$. Cell death type analysis D) A375, E) C32, F) HGF represent the total ratios between cells undergoing extensive DNA fragmentation, intermediate DNA cutting and cells that do not undergo DNA fragmentation. High count of cells with extensive DNA fragmentation corresponds to the high level of late apoptosis, conversely, low fragmentation is considered to be the representation of early apoptosis process $N \in <51, 325>$; the statistic lines directly connecting columns, link both compared groups; the statistic lines above the graph compare all the columns below the line with each other.

4. Discussion

The start point of each tested protocol is the curcumin molecule approaching the cell membrane and binding to its outer leaflet [3]. The molecular dynamics studies, showed no exchange of curcumin between both membrane layers (Figure 2). The result is supported by other research proving that due to the amphipathic structure of curcumin, most of the compound does not migrate between the sides of the membrane but constantly remains in the outer portion [3, 30]. Curcumin remains in the water- membrane interphase and thus without any external factors nor the endocytosis, the drug cannot interact with the cytoplasmic proteins. Thus, the compound interacts only with the membrane proteins and by increasing the average "area per lipid" value (Figure 2) makes the membrane more fluid and fragile [36, 37]. Further, confocal microscopy studies revealed that curcumin is being transported to the intracellular membranes. However, the initial distribution of curcumin varies between cell lines. Namely, curcumin instantly localizes in the intracellular membranes in comparison to melanoma cells, among which the distribution is even in whole cell. In case of C32 cell line, the distribution was somewhere in the middle between even and localized. This could arise from the higher absorption rate of C32 in comparison to A375 and HGF cells. With the time of incubation, the drug shifts towards the intracellular membranes. Localization within the organelles enables the interactions with the composites of cytoplasm [42]. C32 transport curcumin more rapidly than the other cells. The accumulation of curcumin has also been proven by other researchers as well [40]. Transport of the drug is potentially a result of the cellular response to the changes in the membrane stability, by which the cell avoids the disintegration [40]. The probable mechanism of transport is the formation of endosomes with the drug [43]. The accumulation in the membranous structures leads to the interaction of curcumin with organelles, such as mitochondria or endoplasmic reticulum [38, 40]. More light still needs to be shed on mechanisms of drug absorption by cells.

Regarding PDT, there are two options in which curcumin acts. The first involves the absorption of light energy quantum followed by the change of electron structure and the shift to the higher energy level [45]. When the excited compound approaches the potential redox reactant, it passes the energy to the other reagent [46]. However, the pathway occurs only in the presence of compounds susceptible to redox reactivity [45]. The second way is associated with the decomposition of curcumin with the formation of various organic agents (Figure 1B). Molecular dynamics studies proved their release from the membrane due to their hydrophilic properties. The degradation validated in this study (Figure 1B) was observed in the other research as well [17]. Photo-degradation derivatives of curcumin – vanillin, ferulic acid, possess great biological activity [26, 27, 28].

It is widely accepted that hydrophobic compounds are not suitable candidates for electroporation [25]. Thus, nowadays, the researchers try to electroporate cells with curcumin encapsulated in lipid or hydrophilic coatings [47]. This research provides evidence that understanding of the biophysical properties and absorption process of curcumin allows for its application without any additional coatings. However, the cytotoxic level would depend on the properties of the used compound. In the case of melanotic melanoma, the electroporation without any previous incubation with the drug led to the increase in the mitochondrial activity of the cells up to ~120% when the applied electric field was set to 600 V/cm (Figure 8). The acceleration of activity in response to the instant electroporation with curcumin may arise from its even initial distribution in the cells. The other two cell lines were not characterized by this level of rapid increase in mitochondrial activity. The observation correlated with more concentrated distribution of curcumin in fibroblasts and C32 cells. In contrast, the 3 h incubation with curcumin and electroporation afterwards led to a slight reduction of the mitochondrial activity cells. The response of amelanotic melanoma (C32) differed from the melanotic melanoma (A375). Within C32 cells, the mitochondrial activity developed with the incubation time. The situation was more complicated in the case of fibroblasts, which acted like C32 but only with the application of 600 V/cm electric field. However, in 1200 V/cm electric field the mitochondrial activity incremented. Interestingly, the cellular content of curcumin subsided with the increment of electric field when the cells were electroporated with the drug (Figure 6). Therefore, with the application of the electric pulse, curcumin flows out from the cell surface, decreasing its concentration (Figure 1B, 2 and 6). The change in the curcumin content might also arise from the pH-dependent

decomposition of curcumin in the neighborhood of the electrodes. Electrolysis occurring simultaneously with electroporation changes the pH, thus the decrease in the intensity of the curcumin signal, observed on Figure 1C could be a result of the base-mediated decomposition of curcumin into non-ionizable compounds [17]. Obtained results prove that standalone curcumin aided ECT is not a sufficient treatment method, thus it has been excluded from further considerations.

The response to each of the combinational therapies highly depends on the cell line. The first proposed therapy "ECT 0 h, PDT 0 h" affected the mitochondrial activity of the cells, decreasing it by over 80%. The therapy highly induced caspase-12 expression and translocation to the nucleus in HGF and A375 cell lines, thus leading to the activation of DNA-fragmentation activity. However, the activity varied between the cell lines – C32 were most affected with almost 40% of median DNA damage, then A375 with almost 20% and at least affected were fibroblasts – reaching up to 10% of DNA fragmentation. The nuclear content of the caspase-12 in fibroblasts was not as prominent as among melanoma cells. Besides, DNA fragmentation studies indicated that the non-cancerous cells, that remained viable after the therapy were mostly not affected. In the molecular mechanism, in which the "ECT 0 h, PDT 0 h" affects the cells in such a powerful way, this study supports the thesis that electroporation induces the curcumin shift from the outer to the inner leaflet of the cell membrane - where it decomposes to the smaller compounds with high anti-melanoma activity (Figure 1B, 2 and 9). Therefore, the therapy affects all the cells, but both analyzed melanomas undergo extensive apoptosis with DNA fragmentation in contrast to much lower affected fibroblasts.

Due to the relatively low decrease in mitochondrial activity in comparison to other therapies, the "ECT 0 h, PDT 3 h" was considered as inefficient. Moreover, the DNA was not affected to the same extent as the other therapies. The lack of caspase-12 inclusion bodies in the nuclei of the cells, indicated the non-apoptotic death type. No selectivity promoting fibroblasts viability over melanomas was observed. The molecular mechanism of ineffective therapy could be a result of the fast metabolism of curcumin on the cytoplasmic side of the cell membrane or enhanced curcumin absorption (Figure 3). Due to the increased cell metabolism by the initial ECT (Figure 8), the amount of the photosensitizer for PDT diminishes.

The most innovative and never previously described protocol was the "PDT 0 h, ECT 3 h". By affecting melanotic melanoma, the therapy led to the formation of the caspase-12 inclusion bodies in the nuclei of the cells. Caspase-12 expression correlated with the DNA-fragmentation rate reaching up to 50% median and almost 100% for single cases. Due to the lack of effect on the other cell lines - DNA fragmentation of HGF reached the same level as the curcumin-treated cells, and for C32 the level is the same as for the control cells, the protocol was selective towards melanotic melanoma. The cell lines also did not exhibit any caspase bodies in the nuclei, meaning no active caspase-12 was present. The analysis of the cell death type revealed that the A375 melanoma cells died mostly on the late apoptotic pathway. The C32 cell line also showed the late apoptosis induced by the therapy, with the high impact of the early apoptosis process as well. Early apoptosis may be depicted as an even distribution of the caspase throughout the nucleus of the cells but without the formation of the caspase bodies [48]. Altogether, the death-inducing effects are on the much lower level in C32 and HGF cells than among the A375 cell line. The "PDT 0 h, ECT 3 h" therapy effectiveness among melanotic melanoma could be a result of the initial transformation of the curcumin into the ferulic acid and vanillin. High anticancer activity over A375 cell line of the small molecules has already been demonstrated before [26, 28]. The molecular analysis of the therapy among all analyzed cell lines proves that there has to be a mechanism in which the cell absorbs the curcumin degradation products from the extracellular space – by pinocytosis, endocytosis or by the pores formed by oxidized lipids, formed during PDT [46,47]. However, the selectivity towards A375 melanotic melanoma may arise from the interactions of vanillin and ferulic acid with cell-membrane receptors [49]. TRPV vanillin receptor family has already been proved to contribute to cell death among melanotic melanoma (A375) [49, 50]. In this way, the cell could become more sensitive to the electric field, thus the further ECT could enhance the oxidative stress in the carcinoma by the ROS production or induce necrosis by the application of the high-voltage electric field [51, 52, 53]. Undoubtedly, most of the effect was the result of PDT.

The last proposed therapy ("ECT 3 h, PDT 3 h") could also be described as effective. The highest anticancer activity affected C32 amelanotic melanoma. In comparison to the melanotic melanoma and fibroblasts, the cells exhibited high-level diversity in response to the therapy. The DNA-fragmentation reached almost 100% in some cases, but the median value did not differ significantly from the other therapies involving the 3 h incubation time. This could be a result of early apoptosis induction among the cells, that is not correlated with the extensive DNA fragmentation [55]. In the early apoptotic death, the cells prepare for the DNA fragmentation, and thus, the nucleus is full of caspase-12, but no caspase inclusion bodies are already formed [48]. In contrast, the A375 cells DNA content does not differ from the control in the comet assay, even though there may be seen the caspase bodies in the nuclei of the cells. However, the morphology of bodies differs from the standard ones, namely they are smaller and not centrally situated, but rather incrust the nucleus from the outside (Figure 10). Fibroblasts exhibited response similar to C32. In the case of A375 cells, the DNA fragmentation analysis revealed the extensive late apoptotic or necrotic processes (Figure 10). The "ECT 3 h, PDT 3 h" therapy mechanism is similar to the one in "ECT 0 h, PDT 0 h", with the difference that the most of the curcumin is in this case associated with the intracellular membranes and not the plasmalemma. Accumulation of the curcumin at intracellular membranes leads to their disruption and the release of caspase-12 (Figures 3 and 10). The response of fibroblasts differs from the malignant cells by the distribution of caspase-12.

Analysis of the cell response to the therapies led to the conclusion that there has to be a distinction between the selective response of the specific cell line to the introduced compound and the general mechanism of action of the therapies equally affecting the cell lines. Curcumin and the degradation-derivatives did not exhibit any significant role in fibroblasts death induction but rather physically destroy their integrity – by the disruption of the cell membrane integrity. Conversely, the melanoma cells are highly susceptible to curcumin-based therapies as well as vanillin or ferulic acid standalone treatment [28, 26]. The small molecule compounds have been characterized by high activity against melanoma [27]. Therefore, the proposed therapies aim to deliver the vanillin and ferulic acid to the proper cellular compartment.

5. Conclusions

The most effective combinational therapy was the simultaneous electroporation with curcumin with the PDT afterwards. The applied therapy revealed various impact on the metabolic activity of all cell lines, but the DNA fragmentation of normal cells was on a much lower level. The efficacy of the therapy on melanotic melanoma (A375) is associated with the initial irradiation of the cells with curcumin and further 3 h incubation with the products of curcumin degradation. Afterwards applied ECT leads to the selective apoptosis of melanotic melanoma, with a high degree of DNA fragmentation. Nevertheless, for the amelanotic melanoma (C32) the most selective therapy was 3 h incubation with curcumin forwarded by ECT and subsequent PDT.

In summary, the combination of ECT with PDT was proven to be more effective than each of the component therapies alone. High efficacy towards malignant cells demonstrates the potential of curcumin aided PDT with ECT.

Acknowledgments:

The study was supported by Statutory Subsidy Funds of the Department of Molecular and Cellular Biology no. SUB.D260.20.009 and the light microscopy experiments were partially performed in the Screening Laboratory of Biological Activity Test and Collection of Biological Material, Faculty of Pharmacy and the Division of Laboratory Diagnostics, Wroclaw Medical University, supported by the ERDF Project within the Innovation Economy Operational Programme POIG.02.01.00-14-122/09.

References

1. Dhar, G.; Chakravarty, D.; Hazra, J.; Dhar, J.; Poddar, A.; Pal, M.; Chakrabarti, P.; Surolia, A.; Bhattacharyya, B. Actin-curcumin interaction: Insights into the mechanism of actin polymerization inhibition. *Biochemistry* **2015**, *54*, 1132–1143, doi:10.1021/bi5014408.

2. Gupta, A.P.; Khan, S.; Manzoor, M.M.; Yadav, A.K.; Sharma, G.; Anand, R.; Gupta, S. Anticancer Curcumin: Natural Analogues and Structure-Activity Relationship. In *Studies in Natural Products Chemistry*; Elsevier B.V., 2017; Vol. 54, pp. 355–401.

3. Sun, Y.; Lee, C.C.; Hung, W.C.; Chen, F.Y.; Lee, M.T.; Huang, H.W. The bound states of amphipathic drugs in lipid bilayers: Study of curcumin. *Biophys. J.* **2008**, *95*, 2318–2324, doi:10.1529/biophysj.108.133736.

4. Gutiérrez-Gutiérrez, F.; Palomo-Ligas, L.; Hernández-Hernández, J.M.; Pérez-Rangel, A.; Aguayo-Ortiz, R.; Hernández-Campos, A.; Castillo, R.; González-Pozos, S.; Cortés-Zárate, R.; Ramírez-Herrera, M.A.; et al. Curcumin alters the cytoskeleton and microtubule organization on trophozoites of Giardia lamblia. *Acta Trop.* **2017**, *172*, 113–121, doi:10.1016/j.actatropica.2017.04.027.

5. Yadav, V.S.; Mishra, K.P.; Singh, D.P.; Mehrotra, S.; Singh, V.K. Immunomodulatory effects of curcumin. *Immunopharmacol. Immunotoxicol.* **2005**, *27*, 485–497, doi:10.1080/08923970500242244.

6. Vareed, S.K.; Kakarala, M.; Ruffin, M.T.; Crowell, J.A.; Normolle, D.P.; Djuric, Z.; Brenner, D.E. Pharmacokinetics of curcumin conjugate metabolites in healthy human subjects. *Cancer Epidemiol. Biomarkers Prev.* **2008**, *17*, 1411–1417, doi:10.1158/1055-9965.EPI-07-2693.

7. Kotha, R.R.; Luthria, D.L. Curcumin: Biological, pharmaceutical, nutraceutical, and analytical aspects. *Molecules* 2019, *24*.

8. Şueki, F.; Ruhi, M.K.; Gülsoy, M. The effect of curcumin in antitumor photodynamic therapy: In vitro experiments with Caco-2 and PC-3 cancer lines. *Photodiagnosis Photodyn. Ther.* **2019**, *27*, 95–99, doi:10.1016/j.pdpdt.2019.05.012.

9. Leite, D.P.V.; Paolillo, F.R.; Parmesano, T.N.; Fontana, C.R.; Bagnato, V.S. Effects of photodynamic therapy with blue light and curcumin as mouth rinse for oral disinfection: A randomized controlled trial. *Photomed. Laser Surg.* **2014**, *32*, 627–632, doi:10.1089/pho.2014.3805.

10. Ellerkamp, V.; Bortel, N.; Schmid, E.; Kirchner, B.; Armeanu-Ebinger, S.; Fuchs, J. Photodynamic therapy potentiates the effects of curcumin on pediatric epithelial liver tumor cells. *Anticancer Res.* **2016**, *36*, 3363–3372, doi:10.15496/publikation-14547.

11. Buzzá, H.H.; de Freitas, L.C.F.; Moriyama, L.T.; Rosa, R.G.T.; Bagnato, V.S.; Kurachi, C. Vascular effects of photodynamic therapy with curcumin in a chorioallantoic membrane model. *Int. J. Mol. Sci.* **2019**, *20*, doi:10.3390/ijms20051084.

12. Honors, C.N.; Kruger, C.A.; Abrahamse, H. Photodynamic therapy for metastatic melanoma treatment: A review. *Technol. Cancer Res. Treat.* 2018, *17*.

13. Kielbik, A.; Wawryka, P.; Przystupski, D.; Rossowska, J.; Szewczyk, A.; Saczko, J.; Kulbacka, J.; Chwiłkowska, A. Effects of photosensitization of curcumin in human glioblastoma multiforme cells. *In Vivo (Brooklyn).* **2019**, *33*, 1857–1864, doi:10.21873/invivo.11679.

14. Kazantzis, K.T.; Koutsonikoli, K.; Mavroidi, B.; Zachariadis, M.; Alexiou, P.; Pelecanou, M.; Politopoulos, K.; Alexandratou, E.; Sagnou, M. Curcumin derivatives as photosensitizers in photodynamic therapy: photophysical properties and in vitro studies with prostate cancer cells . *Photochem. Photobiol. Sci.* **2020**, *19*, 193–206, doi:10.1039/c9pp00375d.

15. Duse, L.; Pinnapireddy, S.R.; Strehlow, B.; Jedelská, J.; Bakowsky, U. Low level LED photodynamic therapy using

curcumin loaded tetraether liposomes. *Eur. J. Pharm. Biopharm.* **2018**, *126*, 233–241, doi:10.1016/j.ejpb.2017.10.005.

16. Jankun, J.; Wyganowska-Swiatkowska, M.; Dettlaff, K.; JelinSka, A.; Surdacka, A.; Watróbska-Swietlikowska, D.; Skrzypczak-Jankun, E. Determining whether curcumin degradation/condensation is actually bioactivation (Review). *Int. J. Mol. Med.* 2016, *37*, 1151–1158.

17. Schneider, C.; Gordon, O.N.; Edwards, R.L.; Luis, P.B. Degradation of Curcumin: From Mechanism to Biological Implications. In Proceedings of the Journal of Agricultural and Food Chemistry; American Chemical Society, 2015; Vol. 63, pp. 7606–7614.

18. Weaver, J.C. Electroporation: a general phenomenon for manipulating cells and tissues. *J. Cell. Biochem.* **1993**, *51*, 426–35.

19. Mir, L.M. Bases and rationale of the electrochemotherapy. In Proceedings of the IFMBE Proceedings; Springer Verlag, 2007; Vol. 16, p. 622.

20. Hoejholt, K.L.; Jensen, D.; Dalgaard, L.; Bilgin, M.; Nylandsted, J.; Frandsen, K.; Gehl, J. Calcium electroporation and electrochemotherapy for cancer treatment: Importance of cell membrane composition investigated by lipidomics, calorimetry and in vitro efficacy., doi:10.1038/s41598-019-41188-z.

21. Gehl, J.; Sersa, G.; Matthiessen, L.W.; Muir, T.; Soden, D.; Occhini, A.; Quaglino, P.; Curatolo, P.; Campana, L.G.; Kunte, C.; et al. Updated standard operating procedures for electrochemotherapy of cutaneous tumours and skin metastases. *Acta Oncol. (Madr).* **2018**, *57*, 874–882, doi:10.1080/0284186X.2018.1454602.

22. Kiełbik, A.; Szlasa, W.; Saczko, J.; Kulbacka, J. Electroporation-Based Treatments in Urology. *Cancers (Basel).* **2020**, *12*, 2208, doi:10.3390/cancers12082208.

23. Campana, L.G.; Edhemovic, I.; Soden, D.; Perrone, A.M.; Scarpa, M.; Campanacci, L.; Cemazar, M.; Valpione, S.; Miklavčič, D.; Mocellin, S.; et al. Electrochemotherapy – Emerging applications technical advances, new indications, combined approaches, and multi-institutional collaboration. *Eur. J. Surg. Oncol.* 2019, *45*, 92–102.

24. Mali, B.; Jarm, T.; Snoj, M.; Sersa, G.; Miklavcic, D. Antitumor effectiveness of electrochemotherapy: A systematic review and meta-analysis. *Eur. J. Surg. Oncol.* 2013, *39*, 4–16.

25. Delemotte, L.; Tarek, M. Molecular Dynamics Simulations of Lipid Membrane Electroporation Insecticide effect on voltage-gated sodium channel View project TRPV1 activation View project Molecular Dynamics Simulations of Lipid Membrane Electroporation. *Artic. J. Membr. Biol.* **2012**, doi:10.1007/s00232-012-9434-6.

26. Prabhakar, M.M.; Manoharan, S.; Rejitharaji, T.; Selvasundaram, R.; Islam, V.I.H. Ferulic Acid Reduces Cell Viability through Its Apoptotic Efficacy: An In vitro Approach. *Br. J. Med. Med. Res.* **2015**, 612–621.

27. Chou, T.H.; Ding, H.Y.; Hung, W.J.; Liang, C.H. Antioxidative characteristics and inhibition of α-melanocyte-stimulating hormone-stimulated melanogenesis of vanillin and vanillic acid from Origanum vulgare. *Exp. Dermatol.* **2010**, *19*, 742–750, doi:10.1111/j.1600-0625.2010.01091.x.

28. Marton, A.; Kúsz, E.; Kolozsi, C.; Tubak, V.; Zagotto, G.; Buzás, K.; Quintieri, L.; Vizler, C. Vanillin analogues o-vanillin and 2,4,6-trihydroxybenzaldehyde inhibit NFκB activation and suppress growth of A375 human melanoma. *Anticancer Res.* **2016**, *36*, 5743–5750, doi:10.21873/anticanres.11157.

29. Zielichowska, A.; Saczko, J.; Garbiec, A.; Dubińska-Magiera, M.; Rossowska, J.; Surowiak, P.; Choromańska, A.; Daczewska, M.; Kulbacka, J.; Lage, H. The photodynamic effect of far-red range phthalocyanines (AlPc and Pc green) supported by electropermeabilization in human gastric adenocarcinoma cells of sensitive and resistant type. *Biomed. Pharmacother.* **2015**, *69*, 145–152, doi:10.1016/j.biopha.2014.11.017.

30. Choi, Y.H.; Han, D.H.; Kim, S. woo; Kim, M.J.; Sung, H.H.; Jeon, H.G.; Jeong, B.C.; Seo, S. Il; Jeon, S.S.; Lee, H.M.; et al. A randomized, double-blind, placebo-controlled trial to evaluate the role of curcumin in prostate cancer patients with intermittent androgen deprivation. *Prostate* **2019**, *79*, 614–621, doi:10.1002/pros.23766.

31. Ágoston, D.; Baltás, E.; Ócsai, H.; Rátkai, S.; Lázár, P.G.; Korom, I.; Varga, E.; Németh, I.B.; Viharosné, É.D.R.; Gehl, J.; et al. Evaluation of calcium electroporation for the treatment of cutaneous metastases: A double blinded randomised controlled phase II trial. *Cancers (Basel).* **2020**, *12*, doi:10.3390/cancers12010179.

32. Sahl, H.-G.; Pag, U.; Bonness, S.; Wagner, S.; Antcheva, N.; Tossi, A. Mammalian defensins: structures and mechanism of antibiotic activity. *J. Leukoc. Biol.* **2005**, *77*, 466–475, doi:10.1189/jlb.0804452.

33. Saczko, J.; Dominiak, M.; Kulbacka, J.; Chwiłkowska, A.; Krawczykowska, H. A simple and established method of tissue culture of human gingival fibroblasts for gingival augmentation. *Folia Histochem. Cytobiol.* **2008**, *46*, 117–119, doi:10.2478/v10042-008-0017-4.

34. Ali, Z.; Saleem, M.; Atta, B.M.; Khan, S.S.; Hammad, G. Determination of curcuminoid content in turmeric using fluorescence spectroscopy. *Spectrochim. Acta - Part A Mol. Biomol. Spectrosc.* **2019**, *213*, 192–198, doi:10.1016/j.saa.2019.01.028.

35. Schindelin, J.; Arganda-Carreras, I.; Frise, E.; Kaynig, V.; Longair, M.; Pietzsch, T.; Preibisch, S.; Rueden, C.; Saalfeld, S.; Schmid, B.; et al. Fiji: An open-source platform for biological-image analysis. *Nat. Methods* 2012, *9*, 676–682.

36. Abramoff Michael; Magalhães Paulo; Ram S.J. Image Processing with ImageJ. *Biophotonics Int.* **2003**, *11*, 36–42.

37. Collins, A.R. The comet assay. Principles, applications, and limitations. *Methods Mol. Biol.* 2002, *203*, 163–177.

38. Cortés-Gutiérrez, E.I.; Hernández-Garza, F.; García-Pérez, J.O.; Dávila-Rodríguez, M.I.; Aguado-Barrera, M.E.; Cerda-Flores, R.M. Evaluation of DNA single and double strand breaks in women with cervical neoplasia based on alkaline and neutral comet assay techniques. *J. Biomed. Biotechnol.* **2012**, *2012*, 385245, doi:10.1155/2012/385245.

39. Shimoke, K.; Matsuki, Y.; Fukunaga, K.; Matsumura, Y.; Fujita, E.; Sugihara, K.; Nobuhara, M.; Maruoka, H.; Ikeuchi, T.; Kudo, M. Appearance of nuclear-sorted caspase-12 fragments in cerebral cortical and hippocampal neurons in rats damaged by autologous blood clot embolic brain infarctions. *Cell. Mol. Neurobiol.* **2011**, *31*, 795–802, doi:10.1007/s10571-011-9687-0.

40. Hung, W.C.; Chen, F.Y.; Lee, C.C.; Sun, Y.; Lee, M.T.; Huang, H.W. Membrane-thinning effect of curcumin. *Biophys. J.* **2008**, *94*, 4331–4338, doi:10.1529/biophysj.107.126888.

41. Lyu, Y.; Xiang, N.; Mondal, J.; Zhu, X.; Narsimhan, G. Characterization of Interactions between Curcumin and Different Types of Lipid Bilayers by Molecular Dynamics Simulation. *J. Phys. Chem. B* **2018**, *122*, 2341–2354, doi:10.1021/acs.jpcb.7b10566.

42. Moustapha, A.; Pérétout, P.; Rainey, N.; Sureau, F.; Geze, M.; Petit, J.M.; Dewailly, E.; Slomianny, C.; Petit, P. Curcumin induces crosstalk between autophagy and apoptosis mediated by calcium release from the endoplasmic reticulum, lysosomal destabilization and mitochondrial events. *Cell Death Discov.* **2015**, *1*, 15017, doi:10.1038/cddiscovery.2015.17.

43. Nagahama, K.; Utsumi, T.; Kumano, T.; Maekawa, S.; Oyama, N.; Kawakami, J. Discovery of a new function of curcumin which enhances its anticancer therapeutic potency. *Sci. Rep.* **2016**, *6*, 1–14, doi:10.1038/srep30962.

44. Repnik, U.; Česen, M.H.; Turk, B. The endolysosomal system in cell death and survival. *Cold Spring Harb. Perspect. Biol.* **2013**, *5*, a008755, doi:10.1101/cshperspect.a008755.

45. Castano, A.P.; Demidova, T.N.; Hamblin, M.R. Mechanisms in photodynamic therapy: Part one - Photosensitizers,

photochemistry and cellular localization. *Photodiagnosis Photodyn. Ther.* 2004, *1*, 279–293.

46. Kwiatkowski, S.; Knap, B.; Przystupski, D.; Saczko, J.; Kędzierska, E.; Knap-Czop, K.; Kotlińska, J.; Michel, O.; Kotowski, K.; Kulbacka, J. Photodynamic therapy – mechanisms, photosensitizers and combinations. *Biomed. Pharmacother.* 2018, *106*, 1098–1107.

47. Lu, C.H.; Lin, S.H.; Hsieh, C.H.; Chen, W.T.; Chao, C.Y. Enhanced anticancer effects of low-dose curcumin with non-invasive pulsed electric field on PANC-1 cells. *Onco. Targets. Ther.* **2018**, *11*, 4723–4732, doi:10.2147/OTT.S166264.

48. Lisse, T.S.; Thiele, F.; Fuchs, H.; Hans, W.; Przemeck, G.K.H.; Abe, K.; Rathkolb, B.; Quintanilla-Martinez, L.; Hoelzlwimmer, G.; Helfrich, M.; et al. ER stress-mediated apoptosis in a new mouse model of Osteogenesis imperfecta. *PLoS Genet.* **2008**, *4*, doi:10.1371/journal.pgen.0040007.

49. Yang, Y.; Guo, W.; Ma, J.; Xu, P.; Zhang, W.; Guo, S.; Liu, L.; Ma, J.; Shi, Q.; Jian, Z.; et al. Downregulated TRPV1 Expression Contributes to Melanoma Growth via the Calcineurin-ATF3-p53 Pathway. *J. Invest. Dermatol.* **2018**, *138*, 2205–2215, doi:10.1016/j.jid.2018.03.1510.

50. Zheng, J.; Liu, F.; Du, S.; Li, M.; Wu, T.; Tan, X.; Cheng, W. Mechanism for Regulation of Melanoma Cell Death via Activation of Thermo-TRPV4 and TRPV2. *J. Oncol.* **2019**, *2019*, 7362875, doi:10.1155/2019/7362875.

51. Fusi, C.; Materazzi, S.; Minocci, D.; Maio, V.; Oranges, T.; Massi, D.; Nassini, R. Transient receptor potential vanilloid 4 (TRPV4) is downregulated in keratinocytes in human non-melanoma skin cancer. *J. Invest. Dermatol.* **2014**, *134*, 2408–2417, doi:10.1038/jid.2014.145.

52. Davalos, R. V.; Mir, L.M.; Rubinsky, B. Tissue ablation with irreversible electroporation. *Ann. Biomed. Eng.* **2005**, *33*, 223–231, doi:10.1007/s10439-005-8981-8.

53. Vernier, P.T.; Levine, Z.A.; Wu, Y.-H.; Joubert, V.; Ziegler, M.J.; Mir, L.M.; Tieleman, D.P. Electroporating Fields Target Oxidatively Damaged Areas in the Cell Membrane. *PLoS One* **2009**, *4*, e7966, doi:10.1371/journal.pone.0007966.

54. Libardo, M.D.J.; Wang, T.Y.; Pellois, J.P.; Angeles-Boza, A.M. How Does Membrane Oxidation Affect Cell Delivery and Cell Killing? *Trends Biotechnol.* 2017, *35*, 686–690.

55. Basnakian, A.G.; James, S.J. A rapid and sensitive assay for the detection of DNA fragmentation during early phases of apoptosis. *Nucleic Acids Res.* **1994**, *22*, 2714–5, doi:10.1093/nar/22.13.2714.